RSC Advances

Direct synthesis of PEG-encapsulated gold nanoparticles using branched copolymer nanoreactors

Journal:	*RSC Advances*
Manuscript ID:	RA-ART-04-2014-003500.R2
Article Type:	Paper
Date Submitted by the Author:	12-Mar-2014

Complete List of Authors:	Dunlop, Iain; Imperial College London, Department of Materials Ryan, Mary; Imperial College London, Department of Materials Goode, Angela; Department of Materials, Imperial College London, London, UK, Schuster, Carlos; Department of Materials, Imperial College London, London, UK, Terrill, Nicholas; Diamond Light Source, Weaver, Jon; Department of Materials, Imperial College London, London, UK,

ARTICLE TYPE www. rsc.org/xxxxxx | XXXXXXXX

Direct synthesis of PEG-encapsulated gold nanoparticles using branched copolymer nanoreactors†,‡

Iain E. Dunlop,*[a] Mary P. Ryan,[a] Angela E. Goode,[a] Carlos Schuster,[a] Nicholas J. Terrill[b] and Jonathan V.M. Weaver[a,c,‡]

We report a method of directly synthesizing gold nanoparticles that are coated with poly(ethylene glycol) (PEG) for applications in biology and medicine. The particles are grown within the cores of micelle-like structures formed by pH-responsive branched copolymers of poly(ethylene glycol) methacrylate (PEGMA) and 2-diethylamino methacrylate (DEAMA). The process is cheap and scalable, with PEGylated gold particles prepared in two straightforward steps from commercially available monomers and salts. The formation of gold nanoparticles with mean size of 45 Å is confirmed by transmission electron microscopy. Kinetic studies of nanoparticle growth by small-angle X-ray scattering (SAXS) show that the particles form slowly over a period of >17 hours. This process can be modified by exposure to high-intensity X-rays, which cause widespread rapid nucleation leading to a larger number of smaller particles.

1 Introduction

Recent years have seen an explosion of interest in biomedical applications of gold nanoparticles due to their ease of preparation, lack of toxicity and tunable optical properties[1,2]. Proposed applications range from *in vitro* diagnostic assays[3,4] to drug delivery[5,6] and contrast agents for medical imaging[7]. Due to the high ionic strengths and protein concentrations encountered under physiological conditions, nanoparticles for biomedical use are typically sterically stabilized by coating with water-swollen polymer molecules. These polymers are chosen to resist protein adsorption, with the most popular choice being poly(ethylene glycol) (PEG)[8,9]. For medical applications, PEG has the advantage of a substantial history of regulatory approval and use *in vivo*[10]. To facilitate particular applications, PEGylated nanoparticles can be directly functionalized with biological molecules ranging from small molecule drugs[11] to peptides[9,12] and antibodies[13,14].

Nanoparticles designed for biomedical applications are typically prepared via a multistep process: the nanoparticles are first synthesized using a small molecule surfactant as a capping agent, with the surface being polymer-functionalized as a subsequent step[11,12]. In this paper, we synthesise PEGylated gold nanoparticles *within* the cores of micelle-like structures formed by a pH-responsive branched copolymer[15]. The nanoparticle is thus created, already polymer-stabilized, in a single step once the polymer and the gold precursor have been prepared. This minimizes the need for post-synthesis manipulation of the nanoparticles, and gives a significant advantage in terms of cost and scalability.

This approach to single-step preparation of PEGylated gold nanoparticles requires micelle-like structures that combine a PEG corona with a core that both stabilizes the structure and reduces ionic forms of gold. We achieve this using copolymers that combine PEG side-chains with a branched amine-containing backbone that is hydrophobic above its isoelectric point. This hydrophobicity drives the self-assembly of the micelle, while amine groups are known to complex and reduce gold ions[16]. The micelle-like structures formed by these branched copolymers have the advantage that the amount of polymer in the core and corona can be varied independently during the synthesis of the polymer molecules, giving the potential for dial-up control of core and corona properties[15]. This stands in contrast to block copolymer micelles previously used for nanoparticle synthesis[17–22], where the number of molecules in the micelle is controlled by the thermodynamics of self-assembly, meaning that significant trial and error can be required to generate a desired set of properties. The branched copolymers also have the advantage that they are prepared using a straightforward one-pot synthesis without the need for intermediate preparation of precisely controlled block copolymers. Overall, the PEGylated gold nanoparticles are generated in only two reaction steps from readily available commercial monomers and salts and with no complex purification steps. The approach could readily be extended to generate biofunctionalized nanoparticles for biosensing or therapeutic applications, by incorporation of addressable groups such as carboxylic acids into the PEGMA monomer.

In detail, we use branched copolymers, previously reported by Weaver *et al.*[23] that are synthesized by radical copolymerization of an amine-containing monomer, 2-diethylamino methacrylate (DEAMA), and a monomer bear-

† Electronic Supplementary Information (ESI) available: Full SAXS fitting parameters.

Departments of [a]Materials, and [c]Bioengineering, Imperial College London, Exhibition Road, London SW18 4UT, U.K.

[b]Diamond Light Source Ltd., Diamond House, Harwell Science and Innovation Campus, Chilton, Didcot OX11 0DE, U.K.

* E-mail: i.dunlop@imperial.ac.uk

‡ This article is dedicated *in memorium* our late friend and colleague Dr Jonathan Weaver.

ing a pendant PEG chain, poly(ethylene glycol) methacrylate (PEGMA). A bifunctional monomer, ethylene glycol dimethacrylate (EGDMA) is included to generate a branched chain. These molecules exhibit an extended configuration at low pH, when the $-N(CH_2CH_3)_2$ groups of the DEAMA backbone are protonated and thus hydrophilic. At high pH, above its isoelectric point, the DEAMA becomes hydrophobic and forms the core of a micelle-like structure. The corona of this structure is formed by the PEG sidechains, which remain hydrophilic across the range of pH values. A nanogel structure using a related chemistry but with a non-commercial vinylbenzyl-terminated PEG has been reported by Hayashi *et al.*[24].

In this paper, we demonstrate the successful formation of PEGylated gold nanoparticles within these micelle-like branched copolymers. The nanoparticles are synthesized by loading the branched copolymers with gold (III) chloride, which is slowly reduced to metallic gold, with the amine groups of the DEAMA both complexing the gold (III) chloride ions and acting as a reducing agent. The nanoparticles are thus formed already surrounded by a stabilizing PEG layer. To shed light on the mechanisms of particle formation and growth, we have investigated the kinetics of particle formation using dynamic synchotron-based small angle X-ray scattering. This study opens the way for micelle-like branched copolymers to become an important route for high-volume synthesis of PEGylated nanoparticles for biomedical applications.

2 Materials and Methods

2.1 Branched copolymer-templated gold nanoparticle synthesis

The branched copolymer was prepared and characterized as described previously[23]. Briefly, the monomers DEAMA, PEGMA and EGDMA were polymerized in ethanol in the presence of the chain transfer agent 1-thioglycerol (TG), which acts to limit the molecular weight. The polymer was designed as $PEGMA_5-DEAMA_{95}-EGDMA_{15}-TG_{20}$, ^{1}H NMR showed the actual ratio of PEGMA : DEAMA : EGDMA to be $PEGMA_4-DEAMA_{96}-EGDMA_{15.9}$. Molecular weights from gel permeation chromatography: Mn = 24 900 Da, Mw = 57 200 Da (Mw/Mn = 2.29)[23].

To prepare gold nanoparticles, the branched copolymer was dissolved in acidified ultrapure water (adjusted to pH 2-3, below the polymer isoelectric point of $\sim$ pH 7, all pH adjustments used hydrochloric acid and/or sodium hydroxide), and stirred for 1 – 2 hours to ensure complete dissolution. The pH was then adjusted to the desired value for reaction, usually pH 7, and mixed with a solution of gold (III) chloride (Sigma-Aldrich) in ultrapure water adjusted to the same pH. A final polymer concentration of 2.0 mg/ml was used, while the concentration of gold (III) chloride was varied, keeping the molar ratio of $HAuCl_4$: DEAMA < 1. The reaction mixture was stirred for 24 h at room temperature to obtain the desired gold nanoparticles.

2.2 Transmission electron microscopy (TEM)

As-prepared nanoparticle solutions were drop cast on to holey carbon TEM grids and allowed to dry in air. High-resolution TEM images were acquired on an image-corrected FEI Titan 80-300 (S)TEM operated at 80 kV.

2.3 Small angle X-ray scattering (SAXS)

Small-angle X-ray scattering (SAXS) is a gold-standard technique for in situ characterization of solution-phase nanoparticles, combining X-ray wavelengths small enough to directly probe nanoparticle size and shape with the ability to characterize aqueous solutions without drying[25].

SAXS data were collected on the I22 beamline at the Diamond Light Source[26]. I22 is an undulator beamline delivering approximately 10^{12} photons per second in a spot size of 350μm x 250 μm. For these experiments the double crystal monochromator was set to deliver 13.0 keV X-rays. Data were collected on a Pilatus 2M detector[27]. The data were normalized for transmission using the beamstop diode on I22. Fitting was carried out using the SANSView program[28], with the built-in model *SphereModel*:

$$P(q) = \frac{\text{scale}}{V}\left[\frac{3V(\Delta\rho)(\sin(qR) - qR\cos(qR))}{(qR)^3}\right]^2 + \text{background} \quad (1)$$

where $P(q)$ is the form factor, scale is a prefactor proportional to the volume fraction, V is the particle volume, q is the momentum transfer, R is the sphere radius, and $\Delta\rho$ is the difference in scattering length density between the particle and the solvent. A relative measure of the number of particles per unit volume is given by $\left(\text{scale}/R^3\right)$. Polydispersity was modeled using the Schultz distribution[29].

3 Results and Discussion

3.1 Branched copolymer-templated gold nanoparticle synthesis

Gold nanoparticles were synthesized within micelle-like branched copolymers as described in Materials and Methods. Briefly, aqueous solutions of branched copolymer and gold (III) chloride ($HAuCl_4$) were separately adjusted to pH 7, close to the isoelectric point of the polymer, and mixed. The characteristic ruby red color of gold nanoparticles developed and deepened over a period of $\sim$ 24 h. In contrast, there was no visible reaction within 24 hours when polymer and gold

were instead mixed either well above (pH 12) or well below (pH 2 – 3) the amine isoelectric point. The lack of reaction at very high pH may be due to the densely collapsed nature of the completely hydrophobic polymer backbone, meaning that few amine groups are accessible to the gold (III) chloride ions. In contrast, at very low pH, the polymer is extended and the amine groups accessible. However, the amine-induced reduction of gold (III) chloride is not favored at this pH, since the mechanism involves an electron transfer from the amine to the gold as well as the liberation of H+, both of which become unfavorable at low pH when the amine is already protonated[16].

The success of the synthesis was confirmed by transmission electron microscopy (TEM) and ultra-violet-visible spectroscopy (UV-vis). Figure 1 shows a TEM image of gold nanoparticles prepared using this method. High-resolution images (inset) confirm the crystalline nature of the particles, whose size is in the range c. 20 – 60 Å. The UV-vis spectrum of the gold nanoparticle solution prepared using the branched copolymer shows a single peak at 518 nm, consistent with previous observations of gold nanoparticles[30](Figure 2). TEM images also indicated the presence of an additional population of very small nanoparticles, radius 5 Å or less (top part of Figure 1), however it is unclear whether these are an artefact formed by electron-beam driven reduction of any residual gold (III) chloride, or genuine small nanoparticles such as have been previously reported[31]. Such very small particles would have a negligible effect on the UV-vis spectrum, which would be strongly dominated by the larger particles[32].

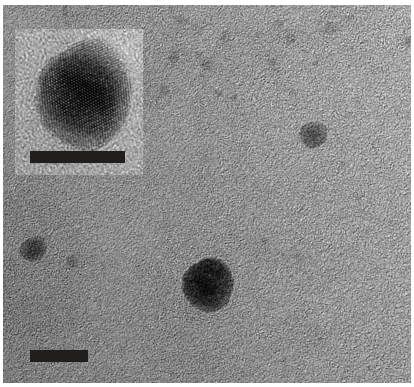

Fig. 1 TEM of gold nanoparticles synthesized in branched copolymer nanoreactors. The main image shows particles deposited on a carbon support film. The inset shows a TEM image of a single particle (scale bars 50 Å).

The particle size distribution was characterized by synchrotron-based small angle X-ray scattering (SAXS). Figure 3a shows the scattered intensity as a function of momentum transfer, q, for a population of branched copolymer-templated gold nanoparticles 19.4 h after the beginning of synthesis. This scattering pattern is well-fitted by assuming a population of polydisperse spheres with mean radius 31 Å. The fit uses a Schultz distribution with a high polydispersity value ($\sigma/x_{\mathrm{mean}} = 0.43$), indicating a broad, right-skewed distribution. This skew towards larger particles is confirmed qualitatively by a histogram of the particle size distribution for the same sample as measured by TEM (Figure 3b); the TEM samples were deposited c. 1 week after the beginning of synthesis and give a larger mean radius of 45 Å indicating that slow particle growth has continued after the 19.4 h time-point of the SAXS measurement. Note that any sub-5 Å. particles present will not be detected by SAXS, since the scattered intensity is dominated by the larger particles.

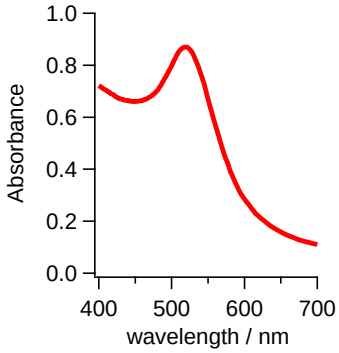

Fig. 2 UV-visible spectrum of branched copolymer-templated gold nanoparticles, showing the characteristic plasmon peak at 518 nm.

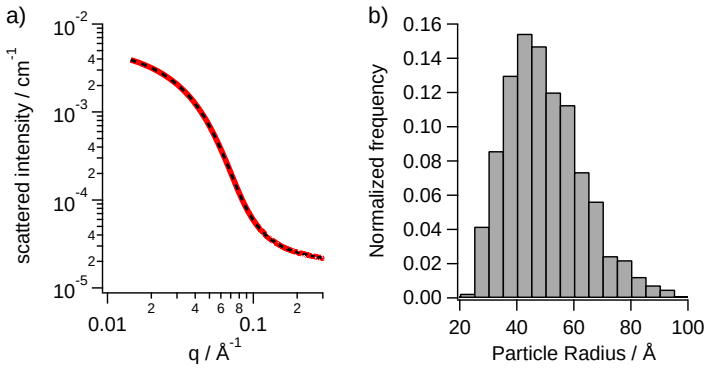

Fig. 3 Size distribution of branched copolymer-templated gold nanoparticles. a) Small angle X-ray scattering from solution following gold nanoparticle formation (—), fitted by a Schultz distribution as described in the text (- -). b) Histogram from TEM image.

Table 1 Comparison of gold nanoparticles synthesized with and without exposure to X-rays. Values are derived from the fits shown in Figure 4, with relative number density (in Arbitary Units) determined as described in the text. Exact reaction time values are given in caption to Figure 4. Stated errors are the uncertainty in fitting.

Molar ratio $HAuCl_4$: DEAMA	Exposure to X-ray beam 10 – 13 h (SAXS)	Mean radius / Å 10 – 13 h (SAXS)	Relative number density / A.U. 10 – 13 h (SAXS)	Mean radius / Å 18 – 20 h (SAXS)	Relative number density / A.U. 18 – 20 h (SAXS)	Mean radius / Å 10 days (TEM)
38%	✓	21 ± 2	9.0^{+3}_{-2}	17 ± 4	13^{+18}_{-6}	-
38%	×	19^{+2}_{-4}	$3.2^{+3.8}_{-0.9}$	31 ± 2	$1.85^{+0.4}_{-0.3}$	45
19%	✓	16^{+2}_{-3}	$6.8^{+5.9}_{-2.0}$	10^{+3}_{-2}	30^{+33}_{-17}	-
19%	×	21 ± 2	$0.8^{+0.3}_{-0.2}$	29 ± 2	0.9 ± 0.2	-

3.2 Kinetics of nanoparticle synthesis and the effect of X-ray exposure

The kinetics of nanoparticle formation were investigated using SAXS, with repeated *in situ* measurements of growing particles. These results were compared with measurements of the same reaction mixture under identical conditions and at the same timepoints, but without exposure to the X-ray beam. The *in situ* samples were exposed to the X-ray beam for 2 mins out of every 15 mins between 1.6 hours and 9.0 hours, giving an overall dose rate of $(1.35 \pm 0.14) \times 10^{15}$ photons $hour^{-1}\,mm^{-2}$ during this period. This frequent irradiation was stopped after 9.0 hours; from this time to 19.4 hours, measurements were taken only infrequently so that the effect of X-ray dose in this later period is likely to be negligible. The precise cumulative dose at each measured time point is given in Supporting Information.

The comparative results are shown in Figure 4 for two different ratios of gold (III) chloride to the charged DEAMA monomer, with parameter values obtained by fitting given in Table 1. In the absence of X-ray exposure, particles grew to c. 15 – 20 Å after 11.1 h, increasing to around 30 Å after 19.4 h. This was true for both higher (38%) and lower (19%) $HAuCl_4$: DEAMA ratios; in the latter case, the lower amount of gold available simply led to a lower number of particles. The number of particles did not measurably increase after the 11 – 13 h time point, and may even have decreased in the case of the higher gold (III) chloride concentration, potentially due to either Ostwald ripening or particle coalescence. For the higher gold concentration (38% ratio), the mean size was measured by TEM as described above after 1 week reaction time and found to be 45 Å, suggesting that particle growth continued even after 19.4 h. These very slow growth kinetics must be a consequence of the templating polymer. Since the DEAMA backbone is expected to strongly complex the gold (III) chloride ions, it is reasonable to expect slow ion diffusion within the polymer core.

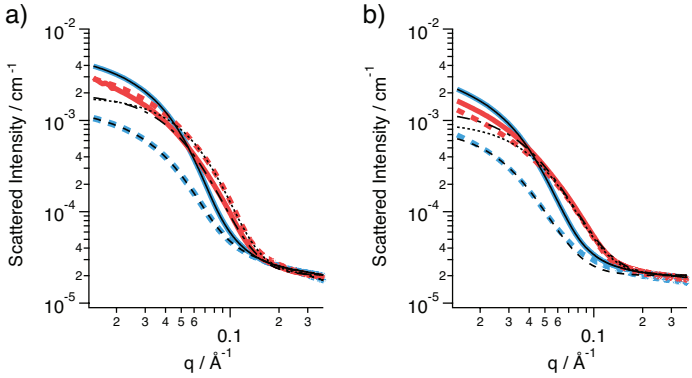

Fig. 4 Kinetics of nanoparticle growth with (red) and without (blue) exposure to X-rays. Small-angle X-ray scattering from reaction solutions with a gold (III) chloride : DEAMA ratio of a) 38% and b) 19%. In both plots, thick red curves show measured scattering with X-ray exposure at time points 12.6 h (▪ ▪) and 18.7 h (▬), and thick blue curves show measured scattering after 11.1 h (▪ ▪) and 19.4 h (▬) without exposure. Thin black lines show corresponding fits to a population of polydisperse spheres, with fitting parameters given in Table 1 and Supporting Information: 12.6 h (·····), 18.7 h (- · - · -) with exposure; 11.1 h (- -) and 19.4 h (——) without exposure.

Exposure to X-rays significantly altered the properties of the particles formed. The final population of particles at the later 18.7 h timepoint consisted of a much larger number of particles than in the non-irradiated case, but of a smaller size (17 ± 4 Å as opposed to 31 ± 2 Å for the 38% $HAuCl_4$: DEAMA sample). This difference is interpreted as being a result of the reduction of the gold (III) chloride by the X-ray beam[33], leading to rapid supersaturation and a corresponding greater number of nucleation events during the period of irradiation prior to 9.0 h. In the absence of X-ray exposure there is less nucleation, leading to a smaller number of particles and eventually a larger size given that the amount of

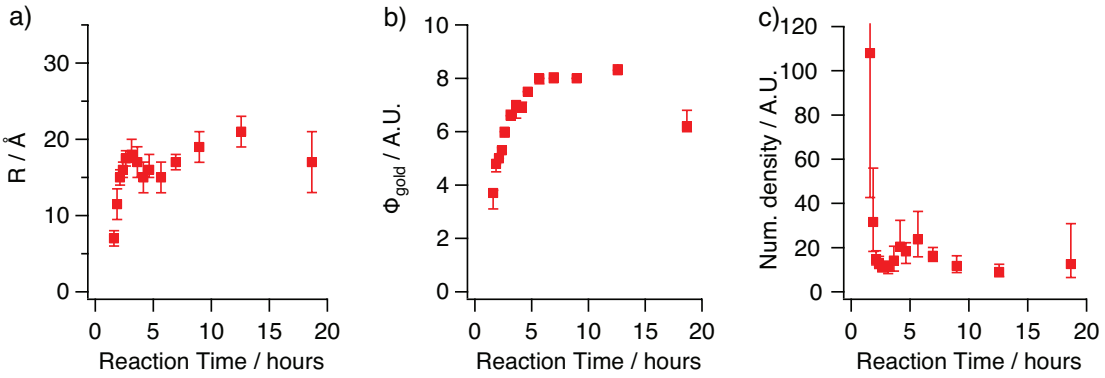

Fig. 6 Extracted data from the dynamic *in situ* SAXS measurements of branched copolymer-templated gold nanoparticle growth: early stage kinetics with a gold (III) chloride : DEAMA ratio of 38% and exposure to X-rays from 1.6 to 9.0 h as described in the text. Plots show a) mean nanoparticle radius, b) relative volume fraction of gold, and c) relative number density as determined from the fits shown in Figure 5. Error bars show the uncertainty in fitting.

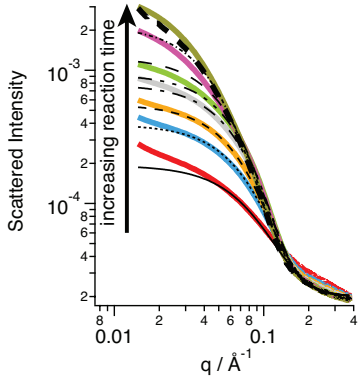

Fig. 5 Dynamic *in situ* SAXS measurements of branched copolymer-templated gold nanoparticle growth: early stage kinetics with a gold (III) chloride : DEAMA ratio of 38% and exposure to X-rays. Thick colored lines show measured data, and thin black lines show corresponding fits. Time points: 1.6 h (,), 1.9 h (,), 2.1 h (,), 2.6 h (,), 3.1 h (,,) 3.6 h ((,), 4.2 h (,). The measured 18.7 h time point (, same as solid red curve in Figure 4) is given for reference.

gold reactant available is finite. The effect of X-ray exposure thus become especially apparent at the later time point (18.7 h) when the supply of gold becomes limiting to the particle size. The idea that X-rays influence the process of nucleation rather than post-nucleation growth is confirmed by the fact that at the earlier 12.6 h time point, the particles were observed to be roughly the same size as those at a similar stage (11.1 h) formed without X-ray exposure. These effects were observed for both gold concentrations measured.

Full kinetic results including early timepoints were determined for the X-ray-exposed case (38% $HAuCl_4$: DEAMA ratio, Figures 5,6). The overall volume of metallic gold is observed to grow steadily, reaching a plateau region around 5-6 h. Most of this increase is due to growth in the particle size, which increases rapidly over the first few hours, from 7 ± 1 Å at 1.6 h to 18^{+2}_{-1} Å at 3.1 h. The number of particles in contrast drops particles drops between 1 – 2 h from an initial high point, indicating either particle coalescence or an Ostwald-type ripening process. Since coalescence is expected to be greatly inhibited by the stabilizing polymer, ripening seems more likely on this short timescale.

4 Conclusions

We have demonstrated the synthesis of PEGylated gold nanoparticles within a pH-responsive branched copolymer nanoreactor. This approach has substantial advantages over traditional multistep processes in terms of scalability, generating stabilized nanoparticles suitable for biomedical applications in only two simple steps from readily available monomers. Particle growth is slow, continuing over > 20 hours, attributable to the retarding influence of the stabilizing polymer. Particle growth kinetics were followed by real-time small-angle X-ray scattering (SAXS). Finally we have compared particles formed under repeated SAXS measurement with particles formed under identical conditions in the absence of X-rays. Exposure to X-rays results in smaller ultimate particle size and greater particle number due to X-ray induced reduction of the gold (III) chloride precursor.

Acknowledgements

TEM image analysis was performed by Tiesheng Wang. This work was carried out with the assistance of the DIAMOND

Light Source (proposal number SM7775). We thank Olga Shebanova and Karla-Luise Herpoldt for assistance during synchrotron beamtime. AEG acknowledges funding provided by EPSRC Science and Innovation Programme: EP/D063329.

References

1 E. C. Dreaden, A. M. Alkilany, X. Huang, C. J. Murphy and M. A. El-Sayed, *Chem. Soc. Rev.*, 2012, **41**, 2740–79.

2 A. S. Thakor, J. Jokerst, C. Zavaleta, T. F. Massoud and S. S. Gambhir, *Nano Lett.*, 2011, **11**, 4029–36.

3 X. Xu, M. S. Han and C. A. Mirkin, *Angew. Chem. Int. Ed. Engl.*, 2007, **46**, 3468–70.

4 R. de la Rica, D. Aili and M. M. Stevens, *Adv. Drug Delivery Rev.*, 2012, **64**, 967–978.

5 H. Jang, S. R. Ryoo, K. Kostarelos, S. W. Han and D. H. Min, *Biomaterials*, 2013, **34**, 3503–10.

6 F. Lu, T. L. Doane, J. J. Zhu and C. Burda, *Inorganica Chimica Acta*, 2012, **393**, 142–153.

7 D. Xi, S. Dong, X. X. Meng, Q. H. Lu, L. J. Meng and J. Ye, *RSC Adv.*, 2012, **2**, 12515–12524.

8 C. D. Walkey, J. B. Olsen, H. B. Guo, A. Emili and W. C. W. Chan, *J. Amer. Chem. Soc.*, 2012, **134**, 2139–2147.

9 E. Oh, J. B. Delehanty, K. E. Sapsford, K. Susumu, R. Goswami, J. B. Blanco-Canosa, P. E. Dawson, J. Granek, M. Shoff, Q. Zhang, P. L. Goering, A. Huston and I. L. Medintz, *ACS Nano*, 2011, **5**, 6434–6448.

10 S. N. S. Alconcel, A. S. Baas and H. D. Maynard, *Polymer Chem.*, 2011, **2**, 1442–1448.

11 F. Wang, Y. C. Wang, S. Dou, M. H. Xiong, T. M. Sun and J. Wang, *ACS Nano*, 2011, **5**, 3679–3692.

12 L. Maus, O. Dick, H. Bading, J. P. Spatz and R. Fiammengo, *ACS Nano*, 2010, **4**, 6617–6628.

13 A. Weiss, T. C. Preston, J. Popov, Q. F. Li, S. Wu, K. C. Chou, H. M. Burt, M. B. Bally and R. Signorell, *J. Phys. Chem. C*, 2009, **113**, 20252–20258.

14 M. Eghtedari, A. V. Liopo, J. A. Copland, A. A. Oraevslty and M. Motamedi, *Nano Lett.*, 2009, **9**, 287–291.

15 M. Oishi, H. Hayashi, T. Uno, T. Ishii, M. Iijima and Y. Nagasaki, *Macromol. Chem. Phys.*, 2007, **208**, 1176.

16 J. D. S. Newman and G. J. Blanchard, *Langmuir*, 2006, **22**, 5882–5887.

17 S. Y. Liu, J. V. M. Weaver, M. Save and S. P. Armes, *Langmuir*, 2002, **18**, 8350–8357.

18 R. C. B. Scaravelli, R. L. Dazzi, F. C. Giacomelli, G. Machado, C. Giacomelli and V. Schmidt, *J. Colloid Interface Sci.*, 2013, **397**, 114–121.

19 J. J. Yuan, A. Schmid, S. P. Armes and A. L. Lewis, *Langmuir*, 2006, **22**, 11022–11027.

20 J. Z. Du, Y. Q. Tang, A. L. Lewis and S. P. Armes, *J. Amer. Chem. Soc.*, 2005, **127**, 17982–17983.

21 T. Ishii, K. Otsuka, H.and Kazunori and Y. Nagasaki, *Langmuir*, 2004, **20**, 561–564.

22 A. Smith, X. Xu, D. Savin and C. McCormick, *Polym. Chem.*, 2010, **1**, 628–630.

23 J. V. M. Weaver, R. T. Williams, B. J. L. Royles, P. H. Findlay, A. I. Cooper and S. P. Rannard, *Soft Matter*, 2008, **4**, 985–992.

24 H. Hayashi, M. Iijima, K. Kataoka and Y. Nagasaki, *Macromolecules*, 2004, **37**, 5389.

25 J. Polte, T. T. Ahner, F. Delissen, S. Sokolov, F. Emmerling, A. F. Thunemann and R. Kraehnert, *J. Amer. Chem. Soc.*, 2010, **132**, 1296–1301.

26 http://www.diamond.ac.uk/Home/Beamlines/small-angle/I22.html.

27 B. Henrich, A. Bergamaschi, C. Broennimann, R. Dinapoli, E. F. Eikenberry, I. Johnson, M. Kobas, P. Kraft, A. Mozzanica and B. Schmitt, *Nucl. Instrum. Methods Phys. Res., Sect. A*, 2009, **607**, 247–249.

28 http://danse.chem.utk.edu/sansview.html.

29 J. S. Higgins and H. C. Benoît, *Polymers and Neutron Scattering*, Oxford University Press, Oxford, U.K., 1994.

30 W. Haiss, N. Thanh, J. Aveyard and D. Fernig, *Anal. Chem.*, 2007, **79**, 4215–4221.

31 M. Schrinner, F. Polzer, Y. Mei, Y. Lu, B. Haupt, M. Ballauff, A. Goldel, M. Drechsler, J. Preussner and U. Glatzel, *Macromol. Chem. Phys.*, 2007, **208**, 1542–1547.

32 S. Malola, L. Lehtovaara, J. Enkovaara and Häkkinen, *ACS Nano*, 2013, **7**, 10263–270.

33 F. Karadas, G. Ertas, E. Ozkaraoglu and S. Suzer, *Langmuir*, 2005, **21**, 437–442.